5.2/5.7-GHz 48-dB Image Rejection GaInP/GaAs HBT Weaver Down-Converter Using LO Frequency Quadrupler

Tzung-Han Wu, *Student Member, IEEE*, and Chinchun Meng, *Member, IEEE*

***Abstract*—A GaInP/GaAs heterojunction bipolar transistor (HBT) down-converter using the Weaver architecture is demonstrated in this paper. The Weaver system is a double-conversion image rejection heterodyne system which requires no bandpass filters in the signal path and no quadrature networks. The Weaver down-converter has the image rejection ratios of 48 dB and 44 dB when the RF frequency is 5.2 GHz and 5.7 GHz, respectively. A new frequency quadrupler is employed in the down-converter to generate the local oscillator (LO) signals. The frequency quadrupler is designed to minimize the phase error when generating LO signals and thus the image rejection performance is improved. A diagrammatic explanation using the complex mixing technique to analyze the image rejection mechanism of the Weaver architecture is developed in this paper. From our analysis, the image rejection can be further improved by making the LO_1 and LO_2 signals coherent.**

***Index Terms*—Complex mixing technique, frequency quadrupler, Gilbert mixer, image rejection, Weaver architecture.**

I. Introduction

THE REJECTION of the image signal is a necessary requirement for the RF receiver design. There already exist several useful architectures to suppress image signals. For example, one of these architectures is the heterodyne system, and the system uses the off-chip SAW image rejection filter to filter out the image signal. There is an obvious drawback that the integration level of the heterodyne system is reduced due to the off-chip SAW filter. Another image rejection architecture is the Hartley low intermediate frequency (low-IF) architecture. The low-IF architecture uses quadrature signals and the multi-section poly-phase filters to filter out the image signals [1], [2]. The low-IF structure can effectively suppress the unwanted image signal; however, many sections of poly-phase filters have to be cascaded in the low-IF system to extend the image rejection bandwidth. Both multi-section passive or active poly-phase filters consume large chip areas. A 5.2-GHz GaInP/GaAs HBT low-IF Hartley down-converter [3] has been demonstrated and the four-section passive poly-phase filter was incorporated to filter out the image signal in the low-IF down-converter. The fabricated chip shows that the IF poly-phase filters occupy many valuable IC estates. Finally, a suitable solution to deal with the image signal is the Weaver architecture [4]–[7]. The Weaver down-converter demonstrated in this paper is implemented using GaInP/GaAs HBT technology. The demonstrated Weaver down-converter has some advantages, such as the semi-insulating substrate and accurate thin-film resistors. The substrate-coupling problem is notorious in the silicon substrate and this drawback may degrade the performance of RFICs. However, the GaInP/GaAs HBT semi-insulating substrate eliminates such a problem and thus good RF performance can be achieved. To the best of our knowledge, the Weaver down-converter with GaInP/GaAs HBT technology is demonstrated for the first time. The integration level of this GaInP/GaAs IC in this work is quite high. The IC contains 166 GaInP/GaAs HBTs.

Although many useful analyses based on trigonometric functions have been employed to explain the image rejection mechanism of the Weaver architecture [5]–[8], a diagrammatic explanation is developed in this paper by using the complex signal-mixing technique [9], [10]. A typical block diagram of the Weaver down-converter is shown in Fig. 1(a).

As shown in Fig. 1(a) and (b), the angular frequencies of the desired RF signal, the unwanted image signal, the LO_1 signal, and the LO_2 signal are denoted as $\omega_{\rm RF}$, $\omega_{\rm IM}$, $\omega_{\rm LO1}$, and $\omega_{\rm LO2}$, respectively. Both LO_1 and LO_2 signals are quadrature signals and the LO_1 frequency is designed to be four times the LO_2 frequency in our work. In addition, the angular frequencies of the output signals that are mixed down by the first-stage mixers are set to be $\omega_{\rm IF1}$, and the angular frequencies of the output signals that are mixed down by the second-stage mixers are denoted as $\omega_{\rm IF2}$. Therefore, the relations among them can be expressed as

$$\begin{aligned} \omega_{\rm IF2} &= \omega_{\rm IF1} - \omega_{\rm LO2} \\ &= \omega_{\rm RF} - \omega_{\rm LO1} - \omega_{\rm LO2} \\ \text{and} \quad \omega_{\rm RF} - \omega_{\rm LO1} &= \omega_{\rm LO1} - \omega_{\rm IM} = \omega_{\rm IF1}. \end{aligned} \tag{1}$$

These two mixers at the first-stage as shown in Fig. 1(a) actually form a complex mixer [9], [10]. The notation LO_1 is changed to LO_1^+ for the following derivations, and the frequency relationship described in (1) is still valid. As shown in Fig. 1(b), the equivalent complex mixer LO_1^+ provides a mixing function of $\exp(j\omega_{\rm LO1}t)$. When the complex LO_1^+ mixes, the spectrum of the RF signal is shifted upwards by a value of $\omega_{\rm LO1}$ as represented in Fig. 2(a) and (b). Furthermore, when the second com-

Manuscript received January 15, 2006; revised July 17, 2006. This work was supported by the National Science Council of Taiwan under contracts NSC 95-2752-E-009-001-PAE and NSC 94-2219-E-009-014, by the Ministry of Economic Affairs of Taiwan under contract 94-EC-17-A-05-S1-020, and by the MoE ATU Program under contract 95W803.

The authors are with the Department of Communication Engineering, National Chiao Tung University, HsinChu, Taiwan, R.O.C. (e-mail: ccmeng@mail.nctu.edu.tw).

Digital Object Identifier 10.1109/JSSC.2006.883332

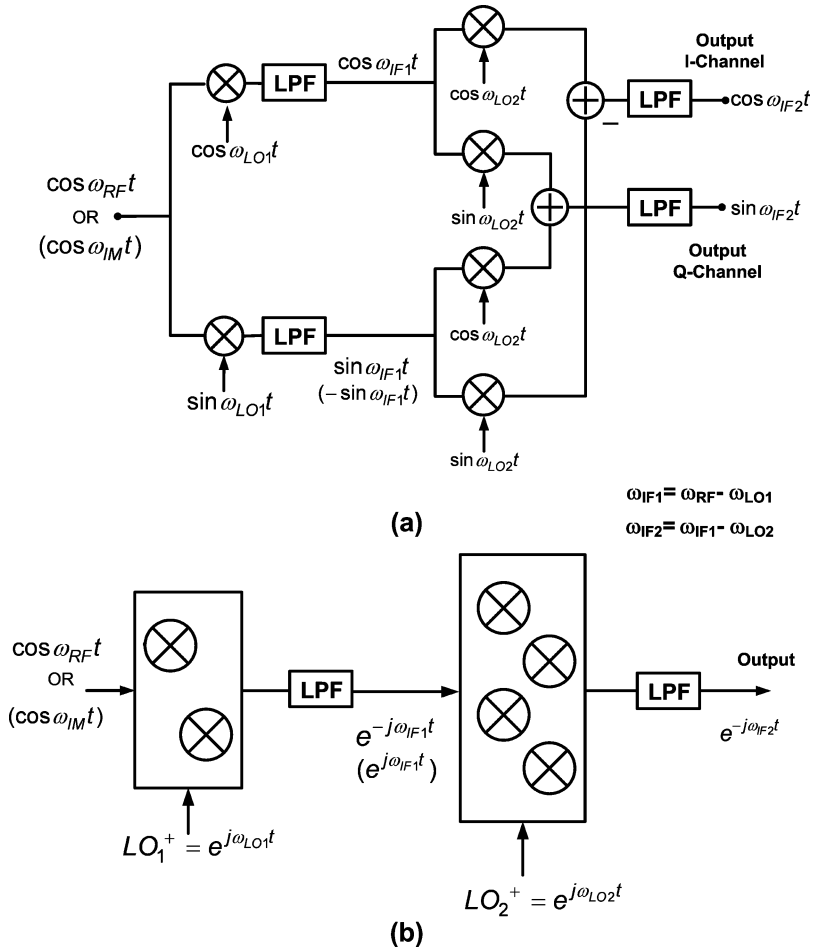

Fig. 1. (a) Block diagram of the Weaver down-converter. (b) Representation of the Weaver architecture using complex signal-mixing approach.

plex mixer LO_2^+ $(\exp(j\omega_{\mathrm{LO2}}t))$ mixes down the signal again, the resulting signal becomes

$$\begin{aligned}&\cos\omega_{\mathrm{RF}}t\times\mathrm{LO}_1^+\times\mathrm{LO}_2^+\\&=\frac{e^{-j\omega_{\mathrm{RF}}t}+e^{j\omega_{\mathrm{RF}}t}}{2}\times e^{j\omega_{\mathrm{LO1}}t}\times e^{j\omega_{\mathrm{LO2}}t}\\&=\frac{e^{-j\omega_{\mathrm{IF1}}t}+e^{j(2\omega_{\mathrm{LO1}}+\omega_{\mathrm{IF1}})t}}{2}\times e^{j\omega_{\mathrm{LO2}}t}\\&=\frac{e^{-j\omega_{\mathrm{IF2}}t}+e^{j(2\omega_{\mathrm{LO1}}+\omega_{\mathrm{LO2}}+\omega_{\mathrm{IF1}})t}}{2}\end{aligned}\tag{2}$$

On the other hand, when the first complex LO_1^+ and the second complex LO_2^+ mix down the unwanted image signal, the output signal can be described as

$$\begin{aligned}&\cos\omega_{\mathrm{IM}}t\times\mathrm{LO}_1^+\times\mathrm{LO}_2^+\\&=\frac{e^{-j\omega_{\mathrm{IM}}t}+e^{j\omega_{\mathrm{IM}}t}}{2}\times e^{j\omega_{\mathrm{LO1}}t}\times e^{j\omega_{\mathrm{LO2}}t}\\&=\frac{e^{-j\omega_{\mathrm{IF1}}t}+e^{j(2\omega_{\mathrm{LO1}}+\omega_{\mathrm{IF1}})t}}{2}\times e^{j\omega_{\mathrm{LO2}}t}\\&=\frac{e^{j(2\omega_{\mathrm{IF1}}-\omega_{\mathrm{IF1}})t}+e^{j(2\omega_{\mathrm{LO1}}+\omega_{\mathrm{LO2}}+\omega_{\mathrm{IF1}})t}}{2}.\end{aligned}\tag{3}$$

The output low-frequency signals of the RF signal and the image signal after mixing down by the two complex mixers are shown in Fig. 2(c). As shown in the figure, the image signal is shifted to the positive frequency while the RF signal is down-converted to the negative frequency in the spectrum. The down-converted RF signal locates at the negative frequency $-\omega_{\mathrm{IF2}}$ while the down-converted unwanted signal locates at the positive frequency $2\omega_{\mathrm{IF1}}-\omega_{\mathrm{IF2}}$. The down-converted image signal is located at the opposite end of the spectrum when compared with the RF signal as shown in Fig. 2(c), and thus the image signal can be easily filtered out either by an IF low-pass filter or by the frequency response of the IF circuits. The diagrammatic explanation of the Weaver architecture give the designer a instinct to design the Weaver system.

A new frequency quadrupler is used to generate LO_1 signals from LO_2 signals. Hence, in practical applications, the circuit demonstrated in this work needs only one low-frequency local oscillator. This frequency planning provides good frequency spacing between LO and RF signals with reasonable circuit complexity. In addition, the low-frequency oscillator is more easily implemented.

II. Diagrammatic Explanation of the Image Rejection Degradation in Weaver Architecture

In this section, an interesting property is obtained to improve the image rejection capability of the Weaver architecture. It is found in this work that when the phase errors of LO_1 and LO_2 are equal, the image rejection ratio can be optimized. The image

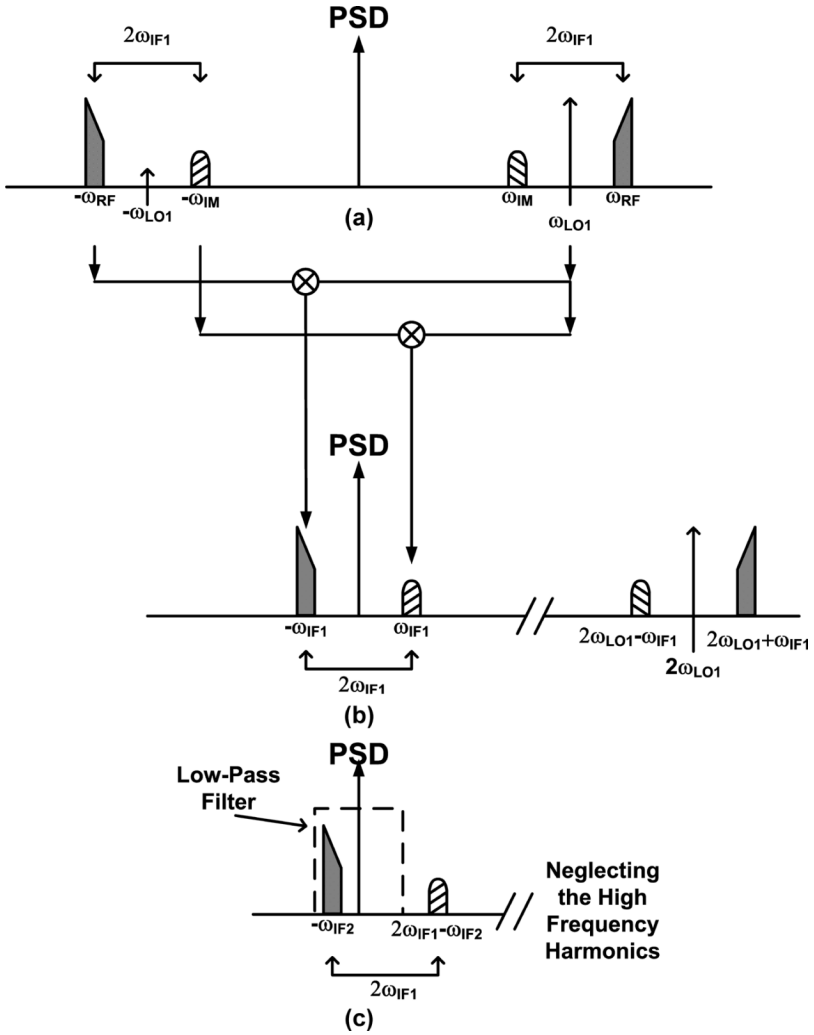

Fig. 2. The spectrum analysis of the Weaver down-converter using the complex mixing analysis. (a) Original RF and image signals before down-conversion. (b) The signals after being down-converted by the first-stage complex mixer. (c) The final signals after being down-converted by the first and second-stage complex mixers.

rejection degradation can be caused by either signal mismatches or circuit mismatches. In order to determine the influences of LO signal mismatches, the diagrammatic explanation is used to analyze this problem. The ideal down-conversion process is shown in Fig. 2 and assuming that the RF and LO signals are perfectly matched without any phase error. Fig. 3 shows a down-conversion process of the Weaver architecture when mismatches are taken into consideration. As shown in Fig. 3(a) and (1), the desired signal is mixed to the IF band by LO_1^+ $(\exp(j\omega_{\mathrm{LO}1}t))$ and LO_2^+ $(\exp(j\omega_{\mathrm{LO}2}t))$ signals that are both in the positive frequency spectrum.

However, when the LO_1 signal becomes slightly mismatched or it contains some phase errors, there will be an LO_1^- signal $(\exp(-j\omega_{\mathrm{LO}1}t))$. The LO_1^- signal is drawn in the dot-line and located in the negative spectrum as shown in Fig. 3(b). The LO_1^- signal arises with the existence of phase errors. The image signal mixed by the LO signal imperfections is shifted to the positive frequency in the spectrum by LO_1^- at first. Next, it is shifted to the negative frequency in the spectrum by the LO_2^+ as shown in Fig. 3(b). The process of the image signal down-converted by the LO_1^- and LO_2^+ can be described as follows:

$$\begin{aligned}
&\text{Image}\left(\text{Down-converted by } \mathrm{LO}_1^- \text{ and } \mathrm{LO}_2^+\right)\\
&\quad = \cos\omega_{\mathrm{IM}}t \times \mathrm{LO}_1^- \times \mathrm{LO}_2^+\\
&\quad = \frac{e^{j\omega_{\mathrm{IM}}t}+e^{-j\omega_{\mathrm{IM}}t}}{2} \times e^{-j\omega_{\mathrm{LO}1}t} \times e^{j\omega_{\mathrm{LO}2}t}\\
&\quad = \frac{e^{-j\omega_{\mathrm{IF}1}t}+e^{j(-2\omega_{\mathrm{LO}1}+\omega_{\mathrm{IF}1})t}}{2} \times e^{j\omega_{\mathrm{LO}2}t}\\
&\quad = \frac{e^{-j\omega_{\mathrm{IF}2}t}+e^{j(-2\omega_{\mathrm{LO}1}+\omega_{\mathrm{IF}1}+\omega_{\mathrm{LO}2})t}}{2}. \qquad (4)
\end{aligned}$$

Comparing (2) and (4), there is an in-band image signal in the IF bandwidth. As illustrated in Fig. 3(c), there is a down-converted unwanted signal caused by the mismatch LO_1^- just located in the same frequency band of the desired signal. As a result, the image rejection ratio is likely to be degraded by the

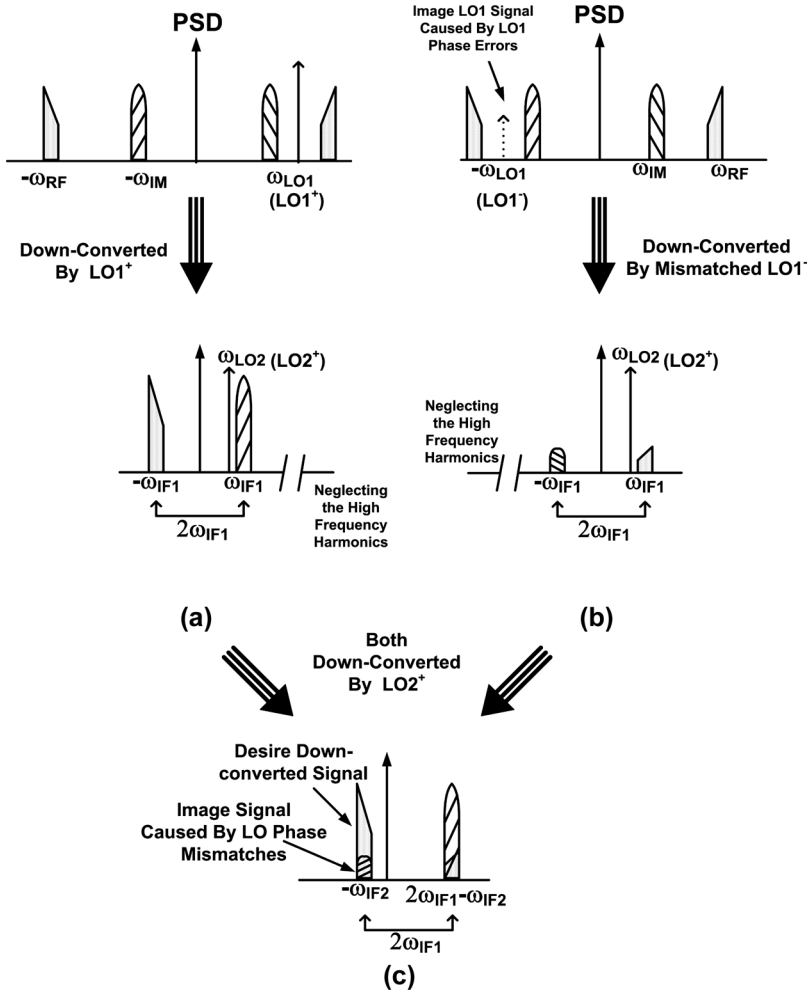

Fig. 3. Spectrum analysis of the Weaver down-converter when the effect of LO_1 and LO_2 signal mismatches are considered. (a) Desired IF signal. (b) Unwanted image signal caused by signal mismatches. (c) Final mixed signals.

signal imperfection as illustrated in these figures. Fig. 3 can visualize the image rejection mechanism of the Weaver architecture. It is important that the image rejection of the Weaver architecture only can be degraded by the signal as shown in (3) when mismatch signals are taken into consideration.

According to previous work [5], the image rejection ratio is influenced by mismatch signals and can be determined by

$$\mathrm{IR(dB)} = 10\log\left[\frac{1+(1+\Delta A)^2+2(1+\Delta A)\cos(\phi_{\varepsilon 1}+\phi_{\varepsilon 2})}{1+(1+\Delta A)^2-2(1+\Delta A)\cos(\phi_{\varepsilon 1}-\phi_{\varepsilon 2})}\right] \tag{5}$$

The coefficient ΔA describes the gain or magnitude mismatches between in-phase and quadrature-phase paths, and the factors $\phi_{\varepsilon 1}$ and $\phi_{\varepsilon 2}$ represent the phase errors of the signals LO_1 and LO_2, respectively [5]. According to (5), it is found that if $\phi_{\varepsilon 1}$ is equal to $\phi_{\varepsilon 2}$, the image rejection performance can be optimized. The detailed derivation of image rejection ratio in the Weaver down-converter is given in Appendix A; the discussion and comparison of image rejection ratio between Weaver and Hartley architectures are also summarized in Appendix A. In our work, no intentional low-pass filter is used and the low-pass function as shown in Fig. 1(a) is achieved sufficiently by the frequency response of the IF circuits. It is because the gain and phase mismatches of the additional low-pass filters caused by the process variation can degrade the image rejection ratio.

Instead of the complicated trigonometric analysis, the diagrammatic explanation of the complex mixing gives the RF designers an instinct to arrange the frequency planning when they design the Weaver image rejection architecture. Consequently, the Weaver receiver can filter out the image signals referred to the frequency of the first LO signal. In our work, the frequency of image signal is 3.1 GHz when the frequency of RF signal is 5.7 GHz and the designed frequency of LO_1 is 4.4 GHz. Similarly, when RF signal is 5.2 GHz and LO_1 equals to 4 GHz, the image signal is 2.8 GHz.

III. Image Rejection Improvement of the Weaver Down-Converter

In this section, a useful technique to improve the image rejection performance of the Weaver down-converter is discussed. As shown in Fig. 1(a), the Weaver architecture requires quadrature LO signals at both LO_1 and LO_2 frequencies in order to eliminate the image signal. Different LO signals can be either generated by two separate local oscillators or by one local oscillator with some circuits that can produce the other LO frequency. Generally speaking, there are two methods to generate different

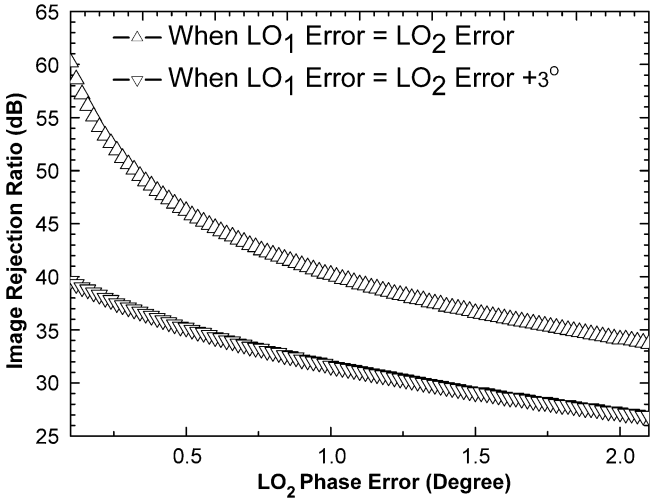

Fig. 4. ADS simulation results of the image rejection ratio influenced by different LO phase mismatches.

LO frequencies with only one LO signal source: frequency dividing or frequency multiplying. The frequency of LO_2 is usually lower than that of LO_1 in a Weaver down-converter, and one possible approach of generating LO signals is to scale the LO_1 frequency down to the LO_2 frequency. In this kind of arrangement, a precise divider circuit is needed not only to scale down the LO frequency but also to generate accurate quadrature signals. Instead of frequency dividing, a frequency multiplying circuit is incorporated to generate the LO signals in this work. Obviously, it is much easier to implement a good low-frequency oscillator than a good high-frequency oscillator in the same technology. In this work, the Weaver down-converter only needs a single low-frequency local oscillator, and a special multiplier is employed to generate the LO_1 signals.

Generating another signal from one local oscillator inevitably produces extra phase error compared with original signals. Both multiplying and dividing processes will distort the generated signal because of the imperfections of the multiplier and divider themselves. Basically, the analog Gilbert multiplier [11] is widely used to multiply signals, and the Gilbert multiplier contains a differential pair and a current commutation Gilbert cell for its two input port. If the time delays between the upper (the Gilbert cell) and lower (the emitter-coupled pair transistors) input ports of the multiplier are considered, there is actually a time delay $\Delta\theta$ between two input signal paths. As a result, the output signal will consist of additional phase errors.

On the other hand, if the multiplier used in this work is able to minimize the time delay when it multiplies, the LO_1 signal will contain much less phase errors. The image rejection can be defined by (5) [5]. Fig. 4 shows a simulation result of image rejection ratio with ideal system components by the ADS (Advanced Design System) harmonic balance simulation. The image rejection ratio is a function of the LO_2 and the LO_1 phase errors. In this simulation, the LO_1 phase error is set to be equal to the LO_2 phase error plus additional 3 degrees error. The other simulation result is that the LO_1 and LO_2 phase errors are set to be equal. As shown in Fig. 4, the image rejection ratio is much larger when the LO_2 phase error is equal to the LO_1 phase error.

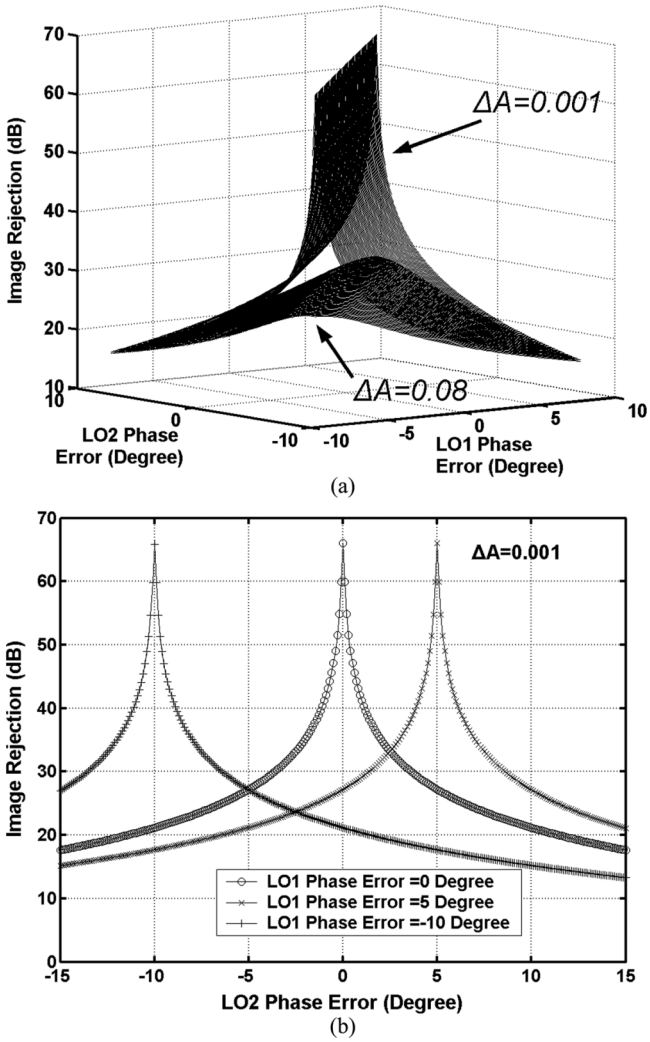

Fig. 5. (a) Simulated image rejection ratio as a function of phase error $\phi_{\varepsilon 2}$ of the LO_2 signal and the phase error $\phi_{\varepsilon 1}$ of the LO_1 signal. (b) Simplified simulated image rejection ratio as a function of LO_1 and LO_2 phase errors.

Fig. 5(a) shows the simulated image rejection ratio as a function of the phase errors $\phi_{\varepsilon 1}$ and $\phi_{\varepsilon 2}$ with gain mismatch, ΔA as a parameter. The maximum image rejection ratio occurs when the LO_1 phase error equals the LO_2 phase error as shown in Fig. 5(a). The image rejection in (5) as a function of the phase error of LO_2 when the gain mismatch and the phase error of LO_1 are fixed is shown in Fig. 5(b). The gain mismatch is fixed to be 0.001, and the phase error of LO_1 is fixed to 0°, 5°, and -10°, respectively. As shown in Fig. 5(b), the maximum image rejection ratio occurs when $\phi_{\varepsilon 1}$ and $\phi_{\varepsilon 2}$ are identical. Therefore, as long as the $\phi_{\varepsilon 1}$ and $\phi_{\varepsilon 2}$ are identical, the image rejection ratio can be maximized.

A time-delay compensated multiplier that will be discussed in the next section can reduce the phase error of LO_1. This fully symmetrical frequency quadrupler circuit is incorporated in this work to generate the LO_1 signal from the LO_2 signal. Compared with the analog Gilbert multiplier, the frequency quadrupler used here can compensate the time delay produced by the multiplier circuit when LO_1 is generated from LO_2. It is worthwhile to mention that the frequency quadrupler employed in this work is useful to improve the image rejection performance. The

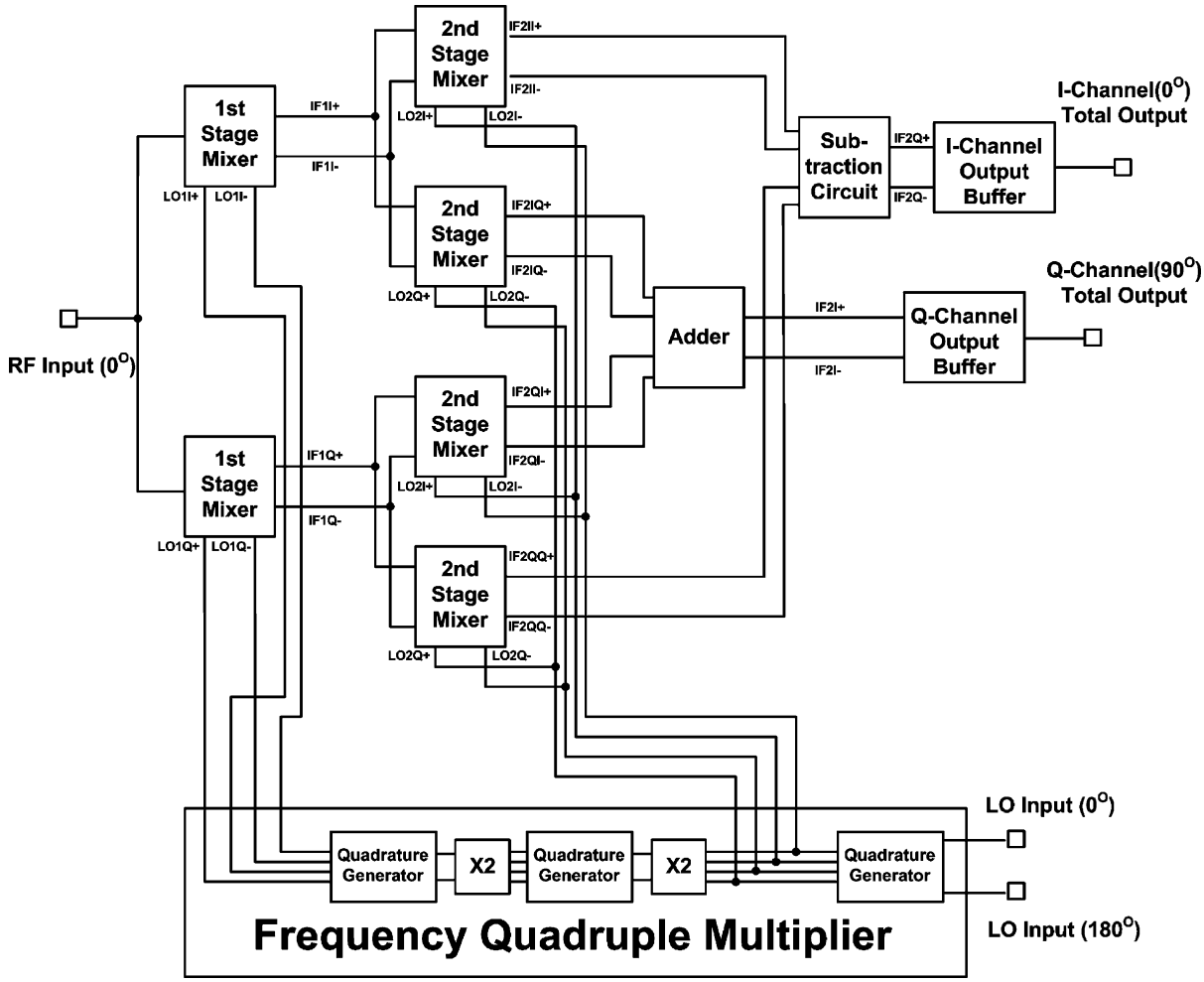

Fig. 6. Total schematic of the 5.2/5.7-GHz GaInP/GaAs HBT 48-dB image rejection Weaver down-converter.

added phase error in the multiplying process is minimized when the frequency quadrupler generates LO_1 signals. As mention in previous section, (5) has a maximum value when $\phi_{\varepsilon 1} = \phi_{\varepsilon 2}$.

Moreover, the quadrature generator used in this work is a multi-section passive poly-phase filter. The poly-phase filters used here are carefully designed to have a reasonable bandwidth to overcome the fluctuation caused by any process variation. Because the GaInP/GaAs technology provides accurate thin-film resistor that helps to fabricate precision resistors, the passive poly-phase filters become more accurate. As a result, the phase error ϕ_1 caused by the quadrature generator can be minimized.

The 5.2- and 5.7-GHz GaInP/GaAs HBT Weaver down-converter has the following frequency planning: 1) When RF signal is 5.7 GHz, the LO_1 signal equals to 4.4 GHz and the LO_2 is 1.1 GHz. 2) When the RF signal is 5.2 GHz, the LO_1 is 4 GHz and the LO_2 is 1 GHz. IF signals are designed always 200 MHz in both cases, and the measured image rejection ratio is 44 dB in case 1, and 48 dB in case 2.

IV. Circuit Design

In this section, the detailed design considerations and trade-offs of each circuit component are discussed individually. In order to facilitate the discussion of each part of the Weaver down-converter, a detailed schematic of the total circuit is shown in Fig. 6.

A. First-Stage Mixer

The circuit topology of the first-stage mixer is shown in Fig. 7. This type of mixer is known as the micromixer [12], [13] for the RF active mixer design.

If the resistance of resistor R_1 and R_3, and the transconductance of transistor Q_5 are properly designed, the input resistance when looking into the RF input port is matched to 50 Ω. The RF input stage of the micromixer is single-ended and the input stage functions as a high-frequency active balun that can be used to generate differential RF currents. A common-collector output buffer is employed to drive the circuits of the next stages. This mixer stage provides about 8-dB conversion gain in simulation when the RF frequency is 5.2 GHz.

B. Second-Stage Mixer

Fig. 8 shows the schematic of the second-stage mixer, and it is a conventional Gilbert mixer [11]. The Gilbert active mixer usually suffers from the slow frequency response of the emitter-coupled pair at the RF input port. The RF input signal of the second-stage mixer has already been down-converted by the first-stage mixer; therefore, the RF input frequency of the

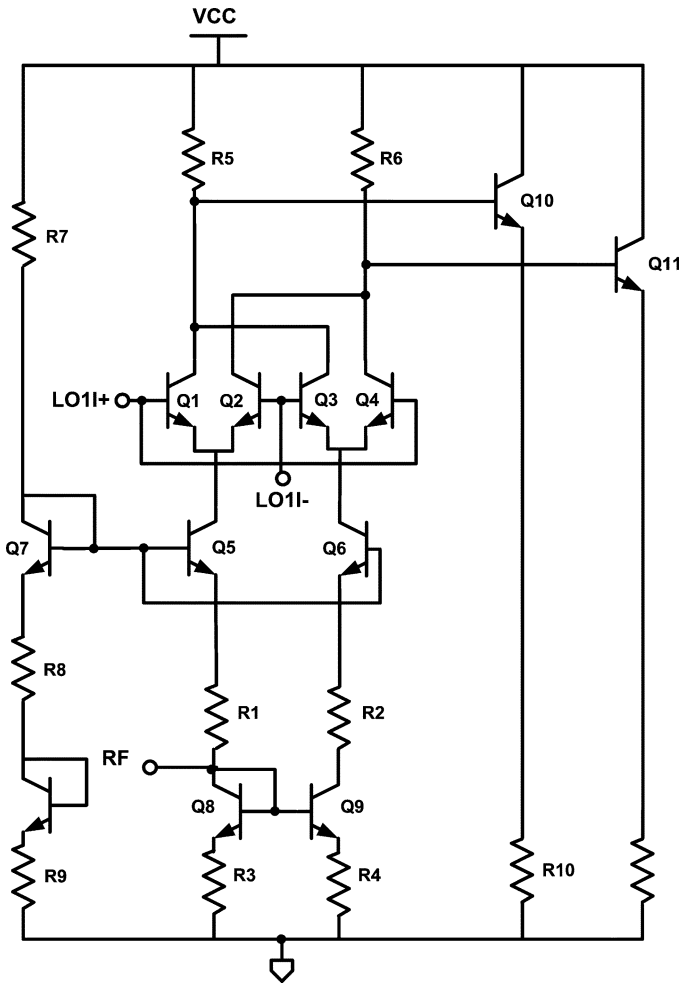

Fig. 7. Schematic of the micromixer used as the first-stage mixer.

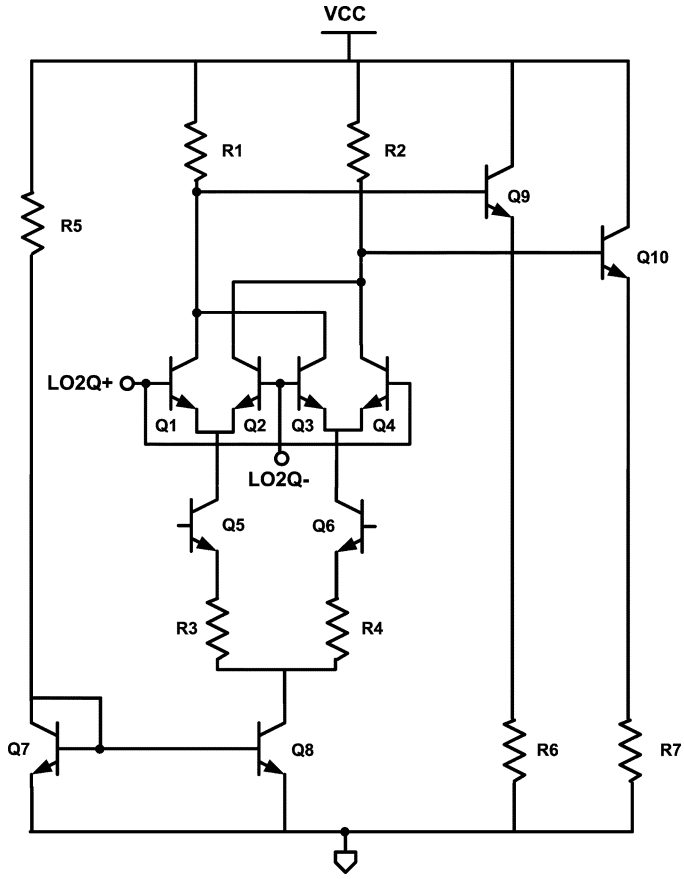

Fig. 8. Schematic of the Gilbert mixer used as the second-stage mixer.

second-stage mixer is much lower than that of the first-stage mixer. Thus, the conventional Gilbert-type active mixers can be used here for the second stage. In order to increase the P_{1dB} of the differential pair, emitter degenerated resistors are added. In the second stage, the mixer must be designed to obtain enough input signal dynamic range. This stage is designed to provide about 7-dB conversion gain in simulation.

C. Analog Adder, Subtraction Circuit, and Output Buffer

For the requirements of addition and subtraction in the complex Weaver architecture, two circuits based on the degenerated differential amplifier are designed: one for addition, and the other for subtraction. As shown in Fig. 9(a), this circuit functions as an adder if the outputs of the two differential amplifiers are directly connected together. This is the current-mode adding technique. However, if the outputs of the differential amplifiers are connected in an anti-phase way, the output currents subtract each other. Fig. 9(b) illustrates a subtraction circuit. In this stage, the down-converted 5.2-GHz RF signals are already amplified about 16 dB by the previous two mixer stages in our simulation. Therefore, the addition and subtraction stages should be designed to prevent the early gain compression. If the signal waveform is clipped, or in other words the waveform is distorted, the image rejection ratio degrades dramatically. In addition, the adder and subtraction circuit also behave as a voltage buffer, and thus the loading effect of the mixers can be reduced.

Fig. 9(c) illustrates the output buffer, which is an asymmetrical differential amplifier with emitter degeneration. This stage is designed to drive the output as well as amplification. The transistor Q_5 as shown in Fig. 9(c) consists of four transistors to increase the output current with reasonable current density.

D. LO Frequency Quadrupler

There are several ways to generate quadrature signals: frequency dividers, the VCO that can directly generate quadrature output signals, and passive *RC* networks. The frequency quadrupler used in this work can generate 4-GHz signals for the first-stage mixer.

The frequency quadrupler consists of two truly-phase-balanced frequency multipliers [14]–[16], three two-section passive poly-phase filters and an output buffer. The poly-phase filters are employed to generate quadrature LO signals and the symmetrical multiplier is used to double the LO signal. First, the external differential LO_2 signals become differential-quadrature after passing through the poly-phase filters. Second, the symmetrical multipliers will double the frequency of the quadrature LO_2.

Repeating the process above, the LO_1 signal can be generated from LO_2 signals. Only one external 1-GHz LO signal is needed in this work when the RF frequency is 5.2 GHz. Because

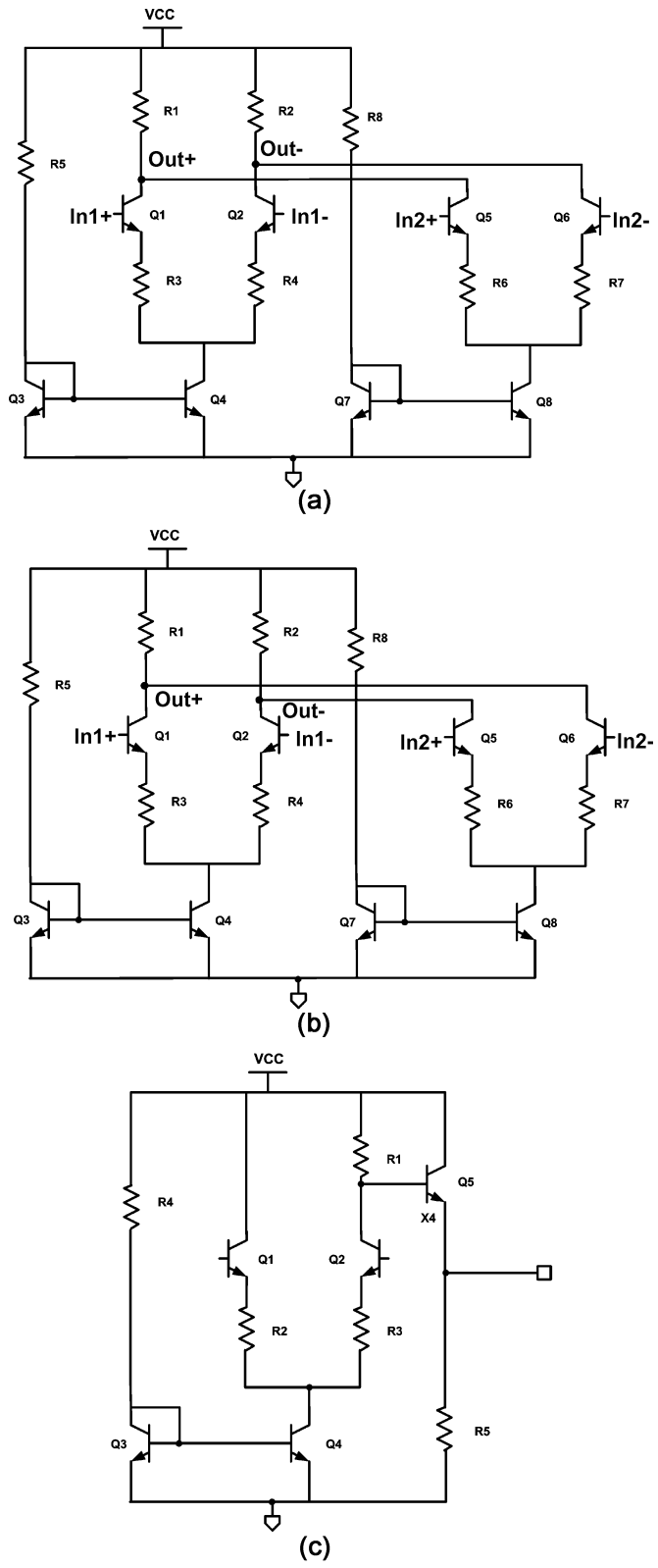

Fig. 9. Schematic of (a) the adder, (b) the subtraction cell, and (c) the output buffer.

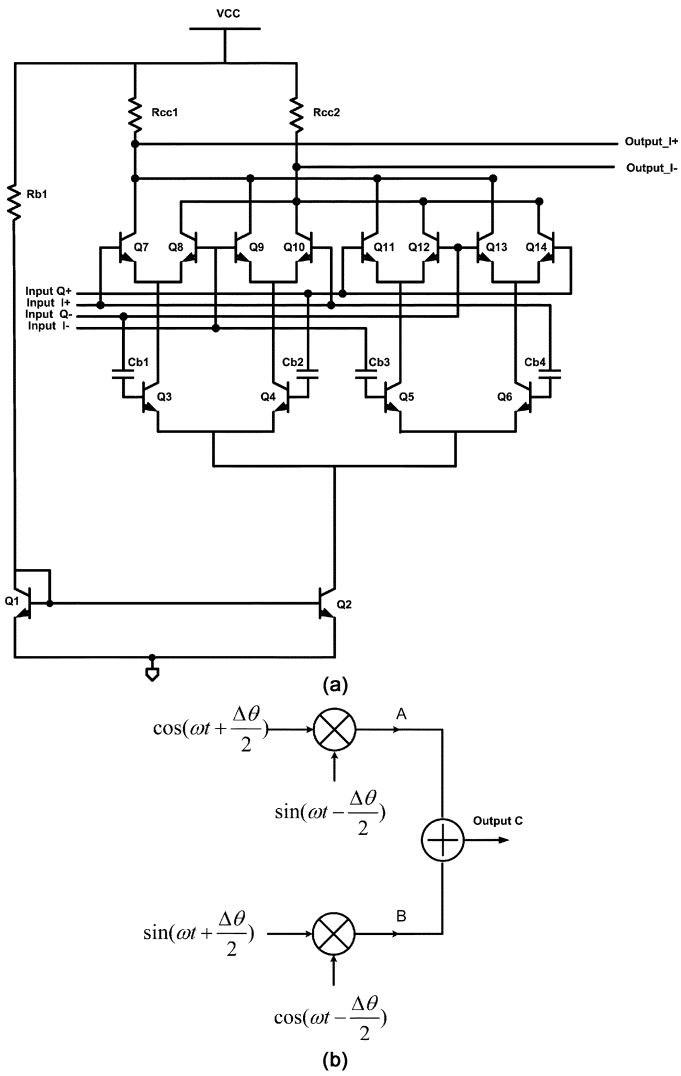

Fig. 10. (a) Schematic of the highly symmetrical frequency multiplier. (b) Block diagram of the multiplier.

the loss caused by the passive poly-phase filters is considerable, each section of the frequency multipliers is designed to provide certain gain to compensate the loss of the passive poly-phase filters. The circuit topology of the truly-phase-balanced frequency multiplier is illustrated in Fig. 10(a). The highly symmetrical multiplier consists of a pair of two conventional multipliers.

One multiplying path contains a phase lead and the other path contains a phase lag, as shown in Fig. 10(b). Thus, the time delays between the upper and lower input stages can be set as a phase lead $-\Delta\theta/2$ and a phase lag $\Delta\theta/2$, respectively. When node A and node B are connected together, the signals contain no additional phase error [14]–[16]. This can be described as

$$\begin{aligned} A &= \cos\left(\omega t + \frac{\Delta\theta}{2}\right) \times \sin\left(\omega t - \frac{\Delta\theta}{2}\right) \\ &= \frac{1}{2}[\sin 2\omega t - \sin\Delta\theta] \\ B &= \sin\left(\omega t + \frac{\Delta\theta}{2}\right) \times \cos\left(\omega t - \frac{\Delta\theta}{2}\right) \\ &= \frac{1}{2}[\sin 2\omega t + \sin\Delta\theta] \\ \therefore\ C &= A + B = \sin 2\omega t. \end{aligned} \tag{6}$$

As a result, the multiplier is suitable for generating accurate high-frequency signals in our work. The frequency quadrupler

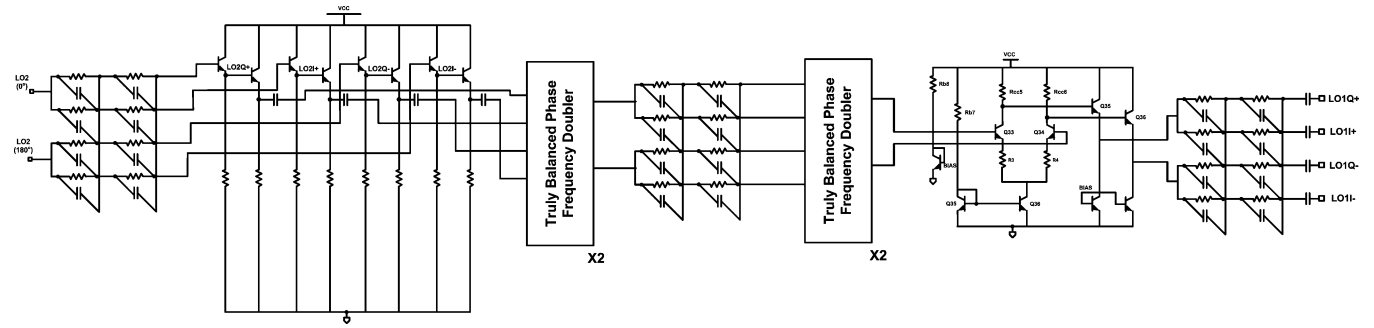

Fig. 11. Schematic of the frequency quadruple multiplier used to correlate the LO_1 and LO_2 signals.

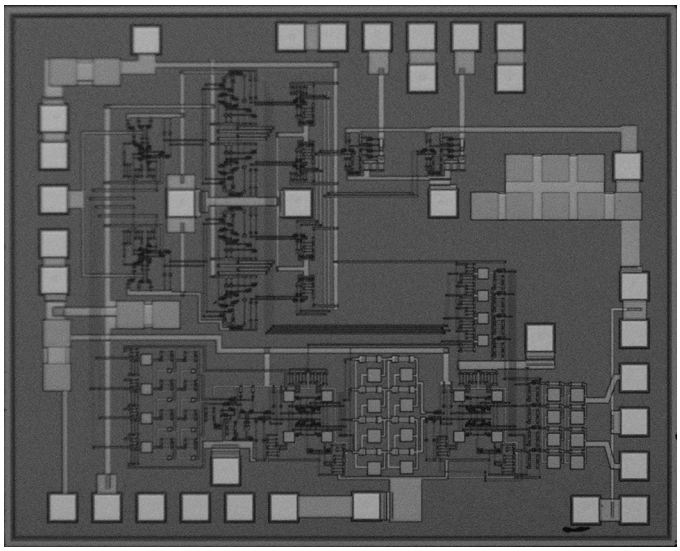

Fig. 12. Die photo of the 5.2/5.7-GHz GaInP/GaAs HBT 48-dB image rejection Weaver down-converter using LO frequency quadruple multiplier.

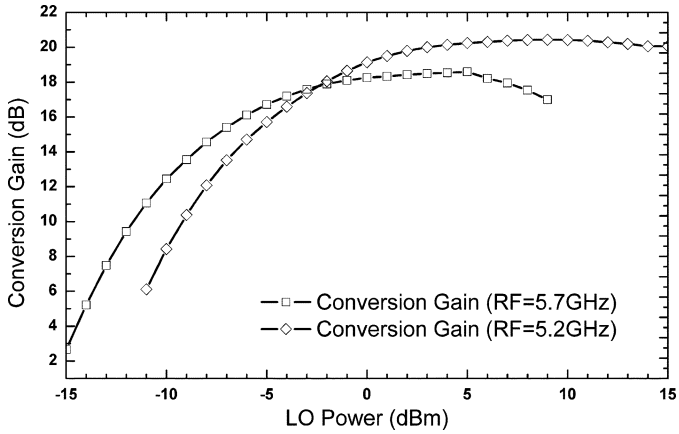

Fig. 13. Measurement results of the conversion gain as a function of LO input power of the Weaver down-converter when input RF frequency is 5.7 GHz and input RF frequency is 5.2 GHz.

is shown in Fig. 11. Using the compensation mechanism of the quadruple frequency multiplier, no extra phase difference of LO_1 and LO_2 caused by the multiplying process occurs, and thus the image rejection is improved. Because the frequency doubler is a wideband multiplier, it is very easy to generate the 4-GHz and 4.4-GHz LO_1 signals. An output buffer is used to drive the LO_1 stage with enough pumping power.

V. Experimental Result and Discussion

Fig. 12 is the die photograph of the demonstrated GaInP/GaAs HBT Weaver down-converter. The total chip size is 2.5 mm $\times$ 2 mm. As shown in Fig. 12, the RF input GSG pad is on the left side of the chip, while the differential LO GSGSG pad is on the right side of the die. The IF output GSGSG pad is on the top of the chip, and DC pads are on the bottom of the die.

The demonstrated Weaver down-converter is fabricated using the 2-μm GaInP/GaAs HBT technology. This HBT process provides the following technical capability. The cutoff frequency of the HBT device is 40 GHz and the $\mathrm{BV_{CEO}}$ is about 11 V. This work is designed using 2 μm $\times$ 2 μm, 2 μm $\times$ 4 μm, and 2 μm $\times$ 6 μm transistors. All of the transistors used in this work are single-emitter, single-base, and single-collector transistors. The DC supply voltage of the Weaver down-convert is 5 V. The measured conversion gain as a function of LO power when the RF $= 5.7$ GHz and the IF $= 200$ MHz is shown in Fig. 13.

As shown in Fig. 13, the peak conversion gain is 18.5 dB for LO powers from 0 to 5 dBm when RF frequency is equal to 5.7 GHz. Fig. 13 also depicts the conversion gain as a function of the LO power when RF frequency is 5.2 GHz and IF frequency is 200 MHz. As shown in Fig. 13, the conversion gain reaches the maximum value (20.5 dB) when the LO power is larger than 4 dBm.

The following section reports the image rejection ratio of the Weaver down-converter when the RF frequency is 5.7 GHz and 5.2 GHz. Because the frequency quadrupler minimizes the phase error of LO_1, the image rejection can be improved as discussed in Fig. 5. The measurement setup is carefully prepared to provide balanced LO signals and thus the intrinsic high image rejection ratio of our work can be demonstrated. In addition, the LO signal paths are well organized, the length of each quadrature LO paths are carefully laid out, and their lengths are made as equal as possible.

Fig. 14 shows the measurement results of the image rejection ratio when the RF input frequency is 5.2 GHz. The measured spectrum shows the IF output power when the desired and image signals are both sent to the RF input port of the Weaver down-converter. As shown in Fig. 14, there is a deliberate 1-MHz offset between the desired and image signals in order to indicate the image rejection ratio in the output IF

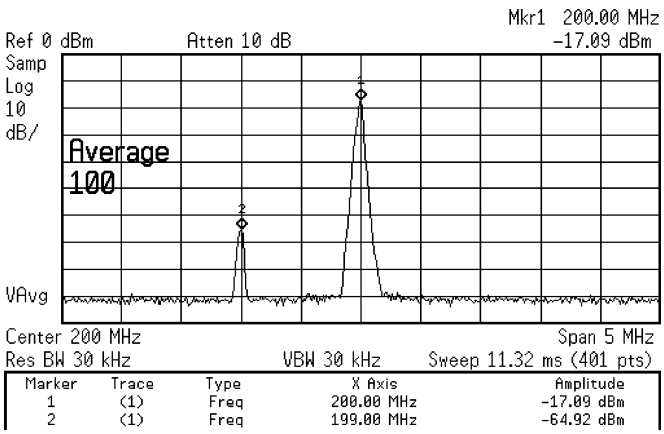

(a)

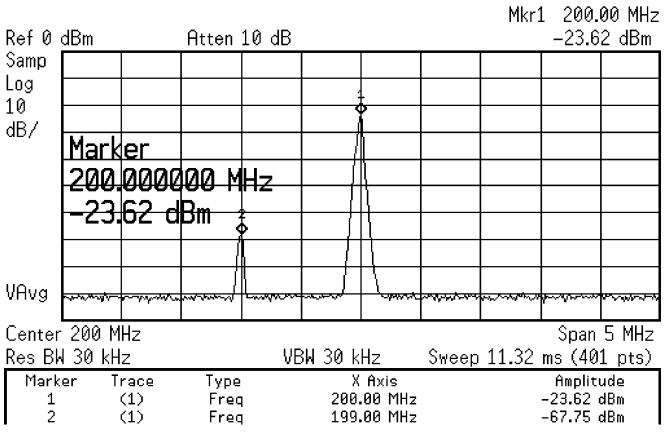

(b)

Fig. 14. Measured image rejection of the proposed Weaver down-converter (a) when the RF frequency is 5.2 GHz and the image signal is 2.8 GHz; (b) when the RF frequency is 5.7 GHz and the image signal is 3.1 GHz.

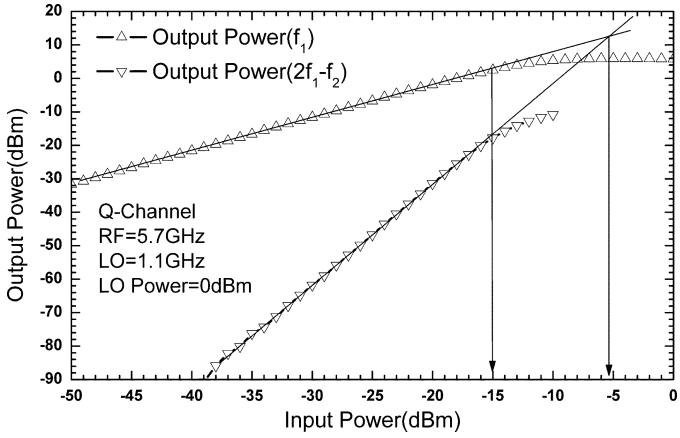

Fig. 15. Measured power performance as a function of RF input power of the Weaver down-converter when RF frequency is 5.7 GHz.

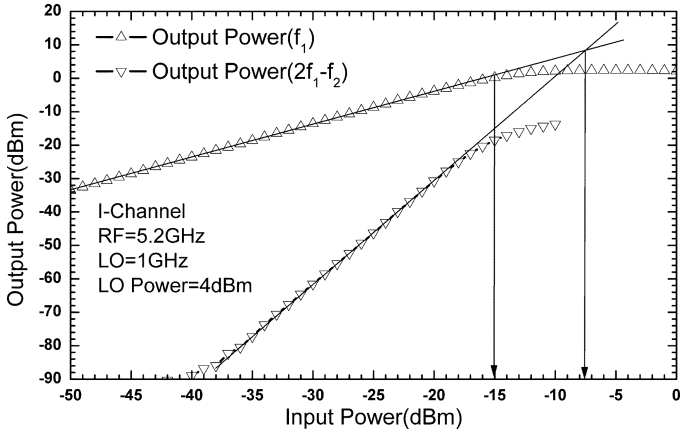

Fig. 16. Measured power performance as a function of RF input power of the Weaver down-converter when RF frequency is 5.2 GHz.

spectrum of the spectrum analyzer. The measurement result indicates that the image rejection ration is 48 dB when the desired signal is 5.2 GHz. Similarly, the image rejection ratio between RF and image signals is about 44 dB when RF input frequency is 5.7 GHz. Balanced external LO_2 signals are applied to the chip by careful calibration. However, there are no on-chip LO_2 signal phase/gain controls and tuning employed in this work. The demonstrated 48-dB image rejection ratio is achieved because the external LO_2 signals are truly balanced and the frequency quadrupler successfully minimizes the phase error. Although the phase error can be successfully minimized by the frequency quadrupler, the gain mismatch still remains. However, the frequency quadrupler in the LO signal path can tolerate the gain mismatch to some degree. The LO Gilbert cell only needs a small LO power for current commutation. Therefore, the image rejection performance is insensitive to the gain mismatch of the frequency quadrupler in the LO path as long as the LO signal is large enough. Thus, the formula (5) can be applied to calculate the gain mismatch of our chip if LO_1 and LO_2 phase errors are zero for the maximum image rejection ratio. The calculated gain mismatch corresponding to 48-dB image rejection ratio is 0.8%.

When the RF frequency is 5.2 GHz (5.7 GHz), the frequency of the secondary image [7], [8] is 4.8 GHz (5.3 GHz). The measurement results showed no secondary image rejection because the demonstrated circuit does not have the capability of filtering out the secondary image. The high-speed analog-to-digital converter together with the digital signal complex filter or the analog polyphase complex filter can be employed to remove the secondary image signal.

The measured power performance as a function of RF input power is shown in Fig. 15 when RF $= 5.7$ GHz and in Fig. 16 when RF $= 5.2$ GHz. The experimental data shows that IP_{1dB} is -15 dBm, IIP_3 is -5 dBm when RF $= 5.7$ GHz and IP_{1dB} is -15 dBm, IIP_3 is -8 dBm when RF $= 5.2$ GHz.

Fig. 17 shows the input return loss of the RF port and the output return loss of the IF port. The input returns loss is better than 16.5 dB from DC to 6 GHz as shown in Fig. 16, and the output return loss is better than 11 dB when the output frequency is 200 MHz.

Fig. 18 shows the RF-to-IF isolations when IF is fixed to 200 MHz and the isolations are better than -40 dB. Fig. 19 shows that the LO-to-IF isolations are about -26 to -30 dB when the LO frequency starts from 0.9 to 1.2 GHz. The LO-to-RF isolation is also illustrated in Fig. 18, and the measurement results indicate that the isolation is better than -72 dB.

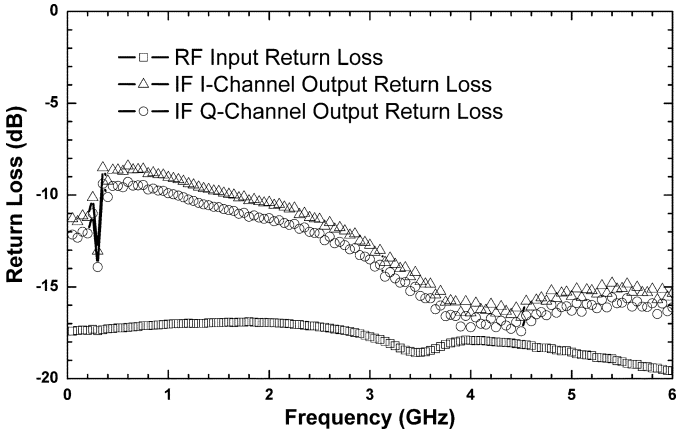

Fig. 17. Measured input and output return losses of the Weaver down-converter.

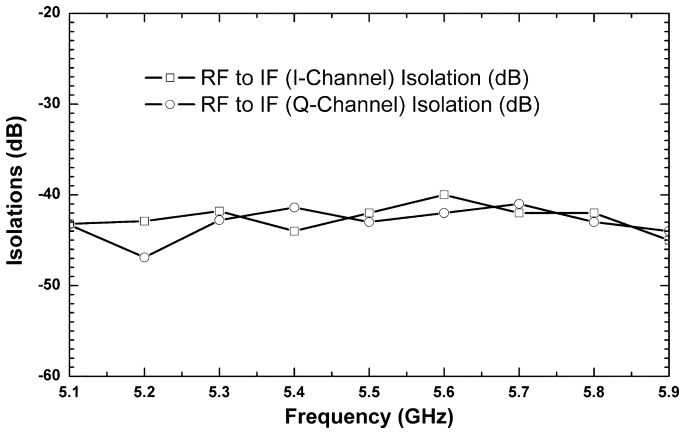

Fig. 18. Measured RF-to-IF isolation for both I-channel and Q-channel of the Weaver down-converter.

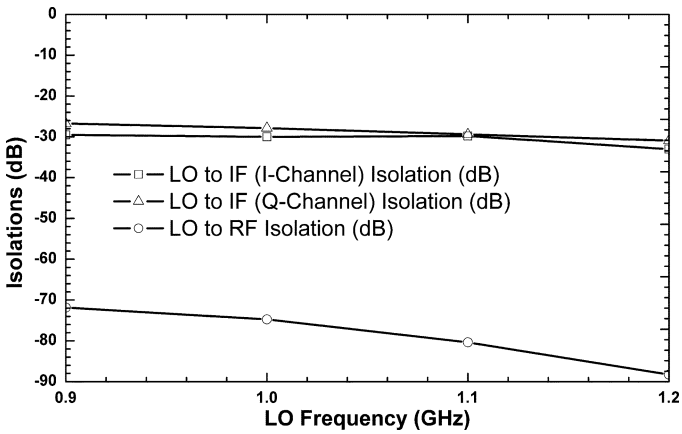

Fig. 19. Measured LO-to-IF and LO-to-RF isolations for both I-channel and Q-channel of the Weaver down-converter.

VI. Conclusion

A diagrammatic explanation using the complex mixing technique to analyze the image rejection mechanism is developed, and a 48-dB image rejection Weaver architecture down-converter when the RF frequency is 5.2 GHz is demonstrated in this paper. The GaInP/GaAs HBT down-converter has 44-dB image rejection ratio when the RF frequency is 5.7 GHz. Both the down-converted IF frequencies are kept the same (200 MHz) by changing the LO input frequencies for the different RF frequency applications. The rejection capability of the image signals of 2.8 and 3.1 GHz is achieved by the Weaver architecture with the LO frequency quadrupler. Because the frequency quadrupler minimizes the phase error when generating LO_2 signals, the LO_1 and LO_2 signals are highly coherent. Consequently, the image rejection ratio is improved.

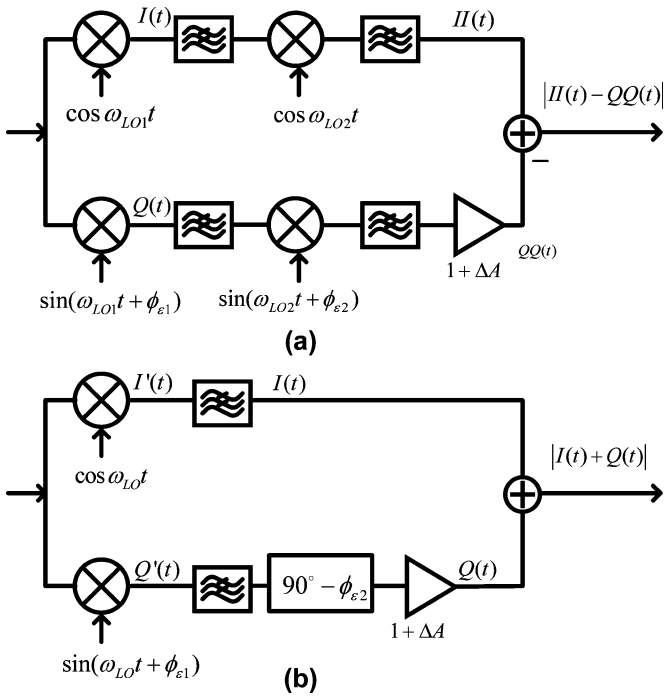

Fig. 20. Block diagram of (a) the Weaver architecture, and (b) the Hartley architecture.

The conversion gain is 20.5 dB when the RF frequency is 5.2 GHz and the conversion gain is 18.5 dB while the RF frequency is 5.7 GHz. The input return loss is better than 16.5 dB from DC to 6 GHz and the output return loss is better than 11 dB when output frequency is 200 MHz. The IP_{1dB} is -15 dBm, the IIP_3 is -5 dBm when RF $= 5.7$ GHz and the IP_{1dB} is -15 dBm, IIP_3 is -8 dBm when RF $= 5.2$ GHz. The RF-to-IF port isolation, the LO-to-IF isolation, and the LO-to-RF isolation are better than -40 dB, -26 dB and -72 dB, respectively.

Appendix A
Mathematical Derivation of Image Rejection Ratio of Weaver and Hartley Architectures

In this section, the detailed derivation of the image rejection ratio is developed. A Weaver down-converter is illustrated in Fig. 20(a). The desired input signal is defined as

$$D(t) = \cos \omega_{\mathrm{RF}} t \tag{7}$$

and the image signal is

$$\mathrm{IM}(t) = \cos \omega_{\mathrm{IM}} t. \tag{8}$$

The $\phi_{\varepsilon 1}$ and $\phi_{\varepsilon 2}$ represent the phase error of the LO_1 and LO_2 signals, respectively. Therefore, the down-converted signals after the first-stage mixer are

$$\begin{aligned} I_D(t) &= \frac{1}{2}\left[\cos(\omega_{\rm RF}-\omega_{\rm LO1})t+\cos(\omega_{\rm RF}+\omega_{\rm LO1})t\right] \\ I_{\rm IM}(t) &= \frac{1}{2}\left[\cos(\omega_{\rm IM}-\omega_{\rm LO1})t+\cos(\omega_{\rm IM}+\omega_{\rm LO1})t\right] \\ Q_D(t) &= \frac{1}{2}\left\{\sin\left[(\omega_{\rm RF}+\omega_{\rm LO1})t+\phi_{\varepsilon 1}\right]\right. \\ &\qquad \left.-\sin\left[(\omega_{\rm RF}-\omega_{\rm LO1})t-\phi_{\varepsilon 1}\right]\right\} \\ Q_{\rm IM}(t) &= \frac{1}{2}\left\{\sin\left[(\omega_{\rm IM}+\omega_{\rm LO1})t+\phi_{\varepsilon 1}\right]\right. \\ &\qquad \left.-\sin\left[(\omega_{\rm IM}-\omega_{\rm LO1})t-\phi_{\varepsilon 1}\right]\right\}. \end{aligned} \tag{9}$$

These signals after the second-stage mixer become

$$\begin{aligned} II_D(t) &= \frac{1}{4}\cos\omega_{\rm IF2}t \\ II_{\rm IM}(t) &= \frac{1}{4}\cos\omega_{\rm IF2}t \\ QQ_D(t) &= -\frac{1}{4}(1+\Delta A) \\ &\quad\times\left[\cos(\phi_{\varepsilon 1}+\phi_{\varepsilon 2})\cos\omega_{\rm IF2}t\right. \\ &\qquad \left.+\sin(\phi_{\varepsilon 1}+\phi_{\varepsilon 2})\sin\omega_{\rm IF2}t\right] \\ QQ_{\rm IM}(t) &= \frac{1}{4}(1+\Delta A) \\ &\quad\times\left[\cos(\phi_{\varepsilon 1}-\phi_{\varepsilon 2})\cos\omega_{\rm IF2}t\right. \\ &\qquad \left.-\sin(\phi_{\varepsilon 1}-\phi_{\varepsilon 2})\sin\omega_{\rm IF2}t\right] \end{aligned} \tag{10}$$

where ΔA represents the gain mismatch. Consequently, the image rejection ratio (IRR) of the Weaver down-converter can be determined as

$$\begin{aligned} \text{IRR(dB)} &= 10\log\frac{|II_D(t)-QQ_D(t)|^2}{|II_{\rm IM}(t)-QQ_{\rm IM}(t)|^2} \\ &= 10\log\left[\frac{1+(1+\Delta A)^2+2(1+\Delta A)\cos(\phi_{\varepsilon 1}+\phi_{\varepsilon 2})}{1+(1+\Delta A)^2-2(1+\Delta A)\cos(\phi_{\varepsilon 1}-\phi_{\varepsilon 2})}\right] \end{aligned} \tag{11}$$

On the other hand, the image rejection ratio of the Hartley down-converter also can be obtained. The block diagram of a Hartley down-converter is shown in Fig. 20(b). If $\phi_{\varepsilon 1}$ represents the phase mismatch of the LO signal, and $\phi_{\varepsilon 2}$ identifies the phase error of the 90° phase shifter (or the poly-phase filter used in the Hartley low-IF systems [1], [10]), the image rejection ratio can be obtained by flowing derivations. The output signals mixed by the first-stage mixer are

$$\begin{aligned} I'_D(t) &= \frac{1}{2}\left[\cos(\omega_D-\omega_{\rm LO})t+\cos(\omega_D+\omega_{\rm LO})t\right] \\ I'_{\rm IM}(t) &= \frac{1}{2}\left[\cos(\omega_{\rm IM}-\omega_{\rm LO})t+\cos(\omega_{\rm IM}+\omega_{\rm LO})t\right] \\ Q'_D(t) &= \frac{1}{2}\left\{\sin\left[(\omega_D+\omega_{\rm LO})t+\phi_{\varepsilon 1}\right]\right. \\ &\qquad \left.-\sin\left[(\omega_D-\omega_{\rm LO})t-\phi_{\varepsilon 1}\right]\right\} \\ Q'_{\rm IM}(t) &= \frac{1}{2}\left\{\sin\left[(\omega_{\rm IM}+\omega_{\rm LO})t+\phi_{\varepsilon 1}\right]\right. \\ &\qquad \left.-\sin\left[(\omega_{\rm IM}-\omega_{\rm LO})t-\phi_{\varepsilon 1}\right]\right\}. \end{aligned} \tag{12}$$

After the 90° phase shifter:

$$\begin{aligned} I_D(t) &= \frac{1}{2}\cos\omega_{\rm IF}t \\ I_{\rm IM}(t) &= \frac{1}{2}\cos\omega_{\rm IF}t \\ Q_D(t) &= \frac{1}{2}(1+\Delta A) \\ &\quad\times\left[\cos(\phi_{\varepsilon 1}+\phi_{\varepsilon 2})\cos\omega_{\rm IF}t\right. \\ &\qquad \left.+\sin(\phi_{\varepsilon 1}+\phi_{\varepsilon 2})\sin\omega_{\rm IF}t\right] \\ Q_{\rm IM}(t) &= -\frac{1}{2}(1+\Delta A) \\ &\quad\times\left[\cos(\phi_{\varepsilon 1}-\phi_{\varepsilon 2})\cos\omega_{\rm IF}t\right. \\ &\qquad \left.-\sin(\phi_{\varepsilon 1}-\phi_{\varepsilon 2})\sin\omega_{\rm IF}t\right] \end{aligned} \tag{13}$$

where $\omega_{\rm IF}=\omega_D-\omega_{\rm LO}=\omega_{\rm LO}-\omega_{\rm IM}$ and ΔA represents the gain mismatch. Therefore, the image rejection ratio of the Hartley architecture is

$$\begin{aligned} \text{IRR(dB)} &= 10\log\frac{|I_D(t)+Q_D(t)|^2}{|I_{\rm IM}(t)+Q_{\rm IM}(t)|^2} \\ &= 10\log\left[\frac{1+(1+\Delta A)^2+2(1+\Delta A)\cos(\phi_{\varepsilon 1}+\phi_{\varepsilon 2})}{1+(1+\Delta A)^2-2(1+\Delta A)\cos(\phi_{\varepsilon 1}-\phi_{\varepsilon 2})}\right] \end{aligned} \tag{14}$$

The image rejection ratio of the Hartley architecture is identical to that of the Weaver architecture as shown in (11) and (14). Furthermore, the image rejection ratio derived in (14) is identical to the result in [8] when the phase shifter or the poly-phase filter is assumed to be fully balanced. From the above derivation, it is clear that eliminating the phase errors or making the phase errors of LO_1 and LO_2 equal can optimize the image rejection ratio of the Weaver down-converter. This property is directly caused by the frequency shifting, as discussed previously. However, the image signal caused by the LO signal and the poly-phase filter mismatches cannot be set to be equal in the Hartley system. The phase error of poly-phase filter obviously is independent from the LO signal of the first-stage mixer in Hartley down-converters. As a result, the image rejection performance of the Weaver architecture has a chance to be further improved by making these individual phase errors coherent.

REFERENCES

[1] F. Behbahani, Y. Kishigami, J. Leete, and A. A. Abidi, "CMOS mixers and polyphase filters for large image rejection," *IEEE J. Solid-State Circuits*, vol. 36, no. 6, pp. 873–887, Jun. 2001.

[2] J. Crols and M. Steyaert, "A single-chip 900-MHz CMOS receiver front-end with a high-performance low-IF topology," *IEEE J. Solid-State Circuits*, vol. 30, no. 12, pp. 1483–1492, Dec. 1995.

[3] C. C. Meng, D. W. Sung, and G. W. Huang, "A 5.2-GHz GaInP/GaAs HBT double-quadrature downconverter with polyphase filters for 40-dB image rejection," *IEEE Microw. Wireless Compon. Lett.*, vol. 15, no. 2, pp. 59–61, Feb. 2005.

[4] D. Weaver, "A third method of generation and detection of single-sideband signals," *Proc. IRE*, pp. 1703–1705, Dec. 1956.

[5] J. C. Rundell, J.-J. Ou, T. B. Cho, G. Chien, F. Brianti, J. A. Weldon, and P. R. Gray, "A 1.9 GHz wide-band IF double conversion CMOS integrated receiver for cordless telephone applications," *IEEE J. Solid-State Circuits*, vol. 32, no. 12, pp. 2071–1088, Dec. 1997.

[6] M. A. I. Elmala and S. H. K. Embabi, "Calibration of phase and gain mismatches in Weaver image-reject receiver," *IEEE J. Solid-State Circuits*, vol. 39, no. 2, pp. 283–289, Feb. 1998.

[7] S. Wu and B. Razavi, "A 900-MHz/1.8-GHz CMOS receiver for dual-band applications," *IEEE J. Solid-State Circuits*, vol. 33, no. 12, pp. 2178–2185, Dec. 1998.

[8] B. Razavi, *RF Microelectronics*. Englewood Cliffs, NJ: Prentice Hall, 1998, pp. 144–146.
[9] J. Crols and M. Steyeart, *CMOS Wireless Transceiver Design*. Dordrecht, The Netherlands: Kluwer Academic, 2000, pp. 52–61.
[10] ——, "Low-IF topologies for high-performance analog front ends of fully integrated receivers," *IEEE Trans. Circuits Syst. II, Analog Digit. Signal Process.*, vol. 45, no. 3, pp. 269–282, Mar. 1998.
[11] B. Gilbert, "A precise four-quadrant multiplier with subnanosecond response," *IEEE J. Solid-State Circuits*, vol. SC-3, no. 4, pp. 365–373, Dec. 1968.
[12] ——, "The MICROMIXER: a highly linear variant of the Gilbert mixer using a bisymmetric class-AB input stage," *IEEE J. Solid-State Circuits*, vol. 32, no. 9, pp. 1412–1423, Sep. 1997.
[13] J. Durec, "An integrated silicon bipolar receiver subsystem for 900 MHz ISM band applications," *IEEE J. Solid-State Circuits*, vol. 33, no. 9, pp. 1352–1372, Sep. 1998.
[14] A. W. Buchwald and K. W. Martin, "High-speed voltage-controlled oscillator with quadrature outputs," *Electron. Lett.*, vol. 27, no. 4, pp. 309–310, Feb. 1991.
[15] A. W. Buchwald, K. W. Martin, A. K. Oki, and K. W. Kobayashi, "A 6-GHz integrated phase-locked loop using AlGaAs/GaAs heterojunction bipolar transistors," *IEEE J. Solid-State Circuits*, vol. 27, no. 12, pp. 1752–1762, Dec. 1992.
[16] R. Magoon, A. Molnar, J. Zachan, G. Hatcher, and W. Rhee, "A single-chip quad-band (850/900/1800/1900 MHz) direct conversion GSM/GPRS RF transceiver with integrated VCOs and fractional-n synthesizer," *IEEE J. Solid-State Circuits*, vol. 37, no. 12, pp. 1710–1720, Dec. 2002.

Tzung-Han Wu (S'06) was born in Taipei, Taiwan, R.O.C., in 1979. He received the B.S. degree with the 1st rank of the class and the M.S. degree from the Department of Electrical Engineering, National Chung-Hsing University, Taichung, Taiwan, in 2001 and 2003, respectively. He worked on GaInP/GaAs HBT, SiGe HBT, and CMOS wideband amplifiers and mixers during his Masters degree study. Currently, he is working toward the Doctorate degree at the Department of Communication Engineering, National Chiao-Tung University, HsinChu, Taiwan.

His current research interests are in the areas of RFICs and MMICs.

Mr. Wu is a member of Phi Tau Phi.

Chin-Chun Meng (M'02) received the B.S. degree in electrical engineering from National Taiwan University, Taipei, Taiwan, R.O.C., in 1985, and the Ph.D. degree in electrical engineering from the University of California, Los Angeles, in 1992.

After completing the Ph.D., he joined the Hewlett Packard Component Group, Santa Clara, CA, in 1993 as a Member of Technical Staff. He is now an Associate Professor in the Department of Communication Engineering at National Chiao Tung University, HsinChu, Taiwan. His current research interests are in the areas of radio frequency integrated circuits (RFIC), high-frequency circuits, and high-speed devices.